Theory and application of the Day plot (M_{rs}/M_s versus H_{cr}/H_c) 2. Application to data for rocks, sediments, and soils

David J. Dunlop

Geophysics, Physics Department, University of Toronto, Toronto, Ontario, Canada

[1]   New theoretical curves relating the hysteresis parameters M_{rs}/M_s and H_{cr}/H_c for single-domain (SD), superparamagnetic (SP), pseudo-single-domain (PSD), and multidomain (MD) grains and their mixtures are applied to published data for natural materials. The Day plot of M_{rs}/M_s versus H_{cr}/H_c has been used to crudely classify samples into box-like SD, PSD, and MD (or sometimes incorrectly, MD + SP) regions with arbitrary boundaries. New type curves for MD, PSD/SD + MD, and SD + SP grains and mixtures permit more subtle and precise modeling. The predicted MD trend and its junction with the PSD trend are observed in two data sets: for magnetite spherules from carbonate rocks and for temperature-varying hysteresis results spanning the Verwey transition. The latter data are the basis of a suggested new method for pinpointing the PSD-MD threshold size. Selected data for pottery clays, soils, and paleosols generally follow SD + MD type curves and indicate intermediate-size PSD magnetite with narrow to broad size distributions. A lake sediment section with known grain-size progression tracks in the predicted sense along the SD + MD trend. Selected data for glaciomarine and pelagic sediments are also generally compatible with SD + MD trends. Examples of remagnetized carbonate rocks, submarine basaltic glasses, and glassy rims of pillow basalts all follow predicted SP + SD or SP + PSD mixing curves, with a large range in volume fraction of SP grains (0–75%) but a narrow range of SP particle sizes: 10 ± 2 nm. Larger SP grains spanning the range to SD size (25–30 nm) are absent for unknown reasons. Oceanic dolerites, gabbros, and serpentinized peridotites in some cases fall in a novel region of the Day plot, parallel to but below magnetite SD + MD mixing curves.   INDEX TERMS: 1540 Geomagnetism and Paleomagnetism: Rock and mineral magnetism; 1594 Geomagnetism and Paleomagnetism: Instruments and techniques; 1533 Geomagnetism and Paleomagnetism: Remagnetization; 1512 Geomagnetism and Paleomagnetism: Environmental magnetism; KEYWORDS: hysteresis parameters, Day plot, remagnetization, submarine basalts, loess, sediment magnetism

1. Introduction

[2]   *Day et al.* [1977] and *Parry* [1982] were the first to graph the ratio of saturation remanence to saturation magnetization, M_{rs}/M_s, against the ratio of remanent coercive force to ordinary coercive force, H_{cr}/H_c. Such a graph has come to be known as a Day plot and is widely used to classify the domain states of paleomagnetic samples. In the companion paper by *Dunlop* [2002] (hereinafter referred to as paper 1), simple theoretical curves are developed for multidomain (MD), superparamagnetic (SP), and single-domain (SD) states and mixtures of states. Pseudo-single-domain (PSD) behavior was modeled as a simple mixture of SD and MD states. Data for (titano)magnetite grains of controlled sizes were generally in good accord with the simplest version of the theory, based on linear approximations to hysteresis and remanent hysteresis curves. Only data for bimodal mixtures of grains with greatly contrasting sizes and magnetic properties required nonlinear hysteresis curves.

[3]   In the present paper, the theoretical curves of paper 1 are compared to data for a wide range of paleomagnetic materials. The examples chosen, which are not necessarily representative of entire classes of sediments or rocks, include pottery (baked clay); modern and ancient soils and loess; lake, shallow marine and pelagic sediments; remagnetized and unremagnetized carbonate rocks, and spherules and other extracts from these rocks; and oceanic pillow basalts, basaltic glasses, dolerites, gabbros, and

peridotites. The data for these samples often follow trends subparallel to but offset from theoretical curves. Earlier interpretations of data trends from carbonate rocks [*Jackson*, 1990; *Channell and McCabe*, 1994; *Suk and Halgedahl*, 1996] and pillow basalts [*Tauxe et al.*, 1996; *Gee and Kent*, 1999] as being due to SD + MD and SP + SD mixtures are confirmed, but data from soils and sediments of many types and from serpentinized peridotites are less readily explained.

2. A Test Spanning the Verwey Transition

[4]   Data for hydrothermally produced magnetites ranging in size from 37 to 760 nm and from 4.6 to 300 μm were compared to theory in paper 1's Figures 3 and 8a and 8b. The first data set lay along the predicted PSD trend and the second lay along the MD trend, but there were no data near the anticipated sharp elbow between these trends around $H_{cr}/H_c \approx 5$, $M_{rs}/M_s \approx 0.02 - 0.03$. The data of *Muxworthy* [1999] fill this gap (Figure 1). Rather than a range of grain sizes, two samples with sizes of 3 and 76 μm delineate the elbow region. A few points for the 3-μm sample fall just outside the envelope of theoretical curves (curve 3 mixes endpoint data for elongated SD and 15-μm magnetites [*Parry*, 1980, 1982]), but otherwise, the predictions of MD and SD + MD modeling are borne out very well. In particular, the reality of a sharp break between PSD and MD trends is confirmed.

[5]   This tracking of the theoretical curves results from temperature variations of the hysteresis parameters. On cooling through
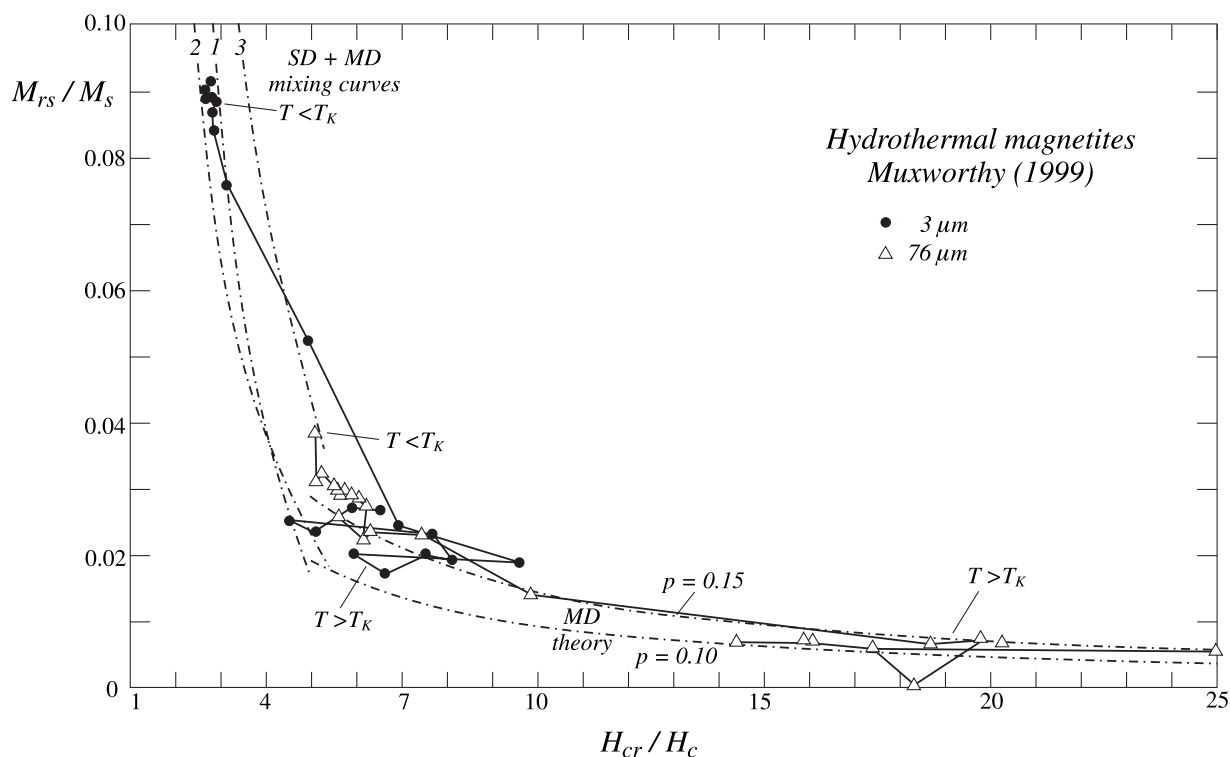
Figure 1. Hysteresis ratios M_{rs}/M_s and H_{cr}/H_c measured at various temperatures above and below the isotropic temperature T_K for hydrothermal magnetites of two sizes, compared with theoretical relations (dot-dashed curves). Both magnetites transform domain state to a smaller effective magnetic grain size at low temperatures.

the Verwey transition, $T_V = 120$ K, H_c in MD crystals increases by an order of magnitude as a result of the large increase in magnetocrystalline anisotropy K [*Özdemir*, 2000]. M_{rs} increases by similar amounts [*Özdemir and Dunlop*, 1999], reflecting a change in domain structure dictated by the harder magnetic properties [*Moloni et al.*, 1996]. Changes also occur at the isotropic temperature $T_K \approx 130$ K, where the anisotropy constant K_1 reverses sign, and to a lesser extent over the entire $100-300$ K range, allowing the PSD-MD transition to be pinpointed. With samples of different grain sizes, the transition size will be reached at different temperatures.

[6] *Muxworthy*'s [1999] 3 μm sample has M_{rs}/M_s and H_{cr}/H_c values that cluster just above the elbow region when $T > T_K$, but migrate rapidly along the PSD curve in cooling through T_V (Figure 1). The PSD threshold size for low-stress hydrothermal magnetites is therefore around 3 μm when temperatures are above T_K. On the other hand, M_{rs}/M_s and H_{cr}/H_c values of the 76-μm sample are well along the MD curve when $T > T_K$ but migrate to a cluster at the MD-PSD elbow in crossing the Verwey transition. The PSD threshold size for the monoclinic phase of magnetite below T_V must therefore be $\approx 70-80$ μm. Further "fine tuning" is limited mainly by the inevitable dispersion of grain sizes in any real sample. Magnetites with higher levels of internal stress, e.g., glass ceramic or crushed and sieved material, will have correspondingly larger PSD threshold sizes, which can be determined in the same way.

[7] The success of this method depends on the model MD and SD + MD curves being themselves temperature independent. The MD relation between M_{rs}/M_s and H_{cr}/H_c is dictated by the internal demagnetizing field $\mathbf{H_d} = -NM_s$. The demagnetizing factor N depends on geometry and M_s is only weakly T-dependent below room temperature. (The equation for the MD Day plot curve, $M_{rs}/M_s \times H_{cr}/H_c = \chi_i H_c/M_s = p$ (equation (3) of paper 1), where χ_i is intrinsic susceptibility, is not obviously temperature insensitive, but it is well known that when H_c increases, χ_i tends

to decrease in the same proportion, since both are governed by the shapes of the potential wells in which domain walls are trapped.) Possible temperature variation of the PSD curve is harder to assess because there is no first-principles equation to work with. This point needs experimental investigation.

3. Data for Pottery (Baked Clays)

[8] The Day plot of Figure 2 includes hysteresis data from *Cui and Verosub* [1995] for six samples of ancient Egyptian (~1350 B.C.) and Greek (~1000 B.C.) pottery, and data from *Yu et al.* [2000] and *Carvallo* [2000] for 35 and 83 samples, respectively, of Ontario native pottery (eight sites, ages from 90 to 1640 A.D.). Despite the diverse origins of the pottery and the clays from which the pots were baked, the data in Figure 2 are concentrated in a small region: $0.15 \leq M_{rs}/M_s \leq 0.30$, $2 \leq H_{cr}/H_c \leq 3$. The points follow the general hyperbolic trend of the model SD + MD mixing curves, most falling somewhat above mixing curve 3 but well below the SD + 10-nm SP mixing curve.

[9] *Carvallo*'s [2000] samples are the most heterogeneous. A subset of points deviates considerably from the normal PSD trend toward high values of both M_{rs}/M_s and H_{cr}/H_c, possibly indicating bimodal SD + MD mixtures (see Figure 12a of paper 1). There are also a few examples (not shown) of truly MD values ($H_{cr}/H_c > 5$, $M_{rs}/M_s < 0.03$). The archeological setting, a floodplain, may account for the coarse-grained fraction in these clays.

[10] On the basis of this admittedly sparse sampling of archeological pottery, *Cui and Verosub*'s [1995] assumption of a broad and continuous magnetic size distribution from SP through SD and into PSD seems reasonable. The SP fraction must be volumetrically small compared to the PSD fraction, however, because the points are not greatly displaced from SD + MD mixing curves. A coarse-grained MD fraction with much softer properties than the main SD-PSD distribution is suggested
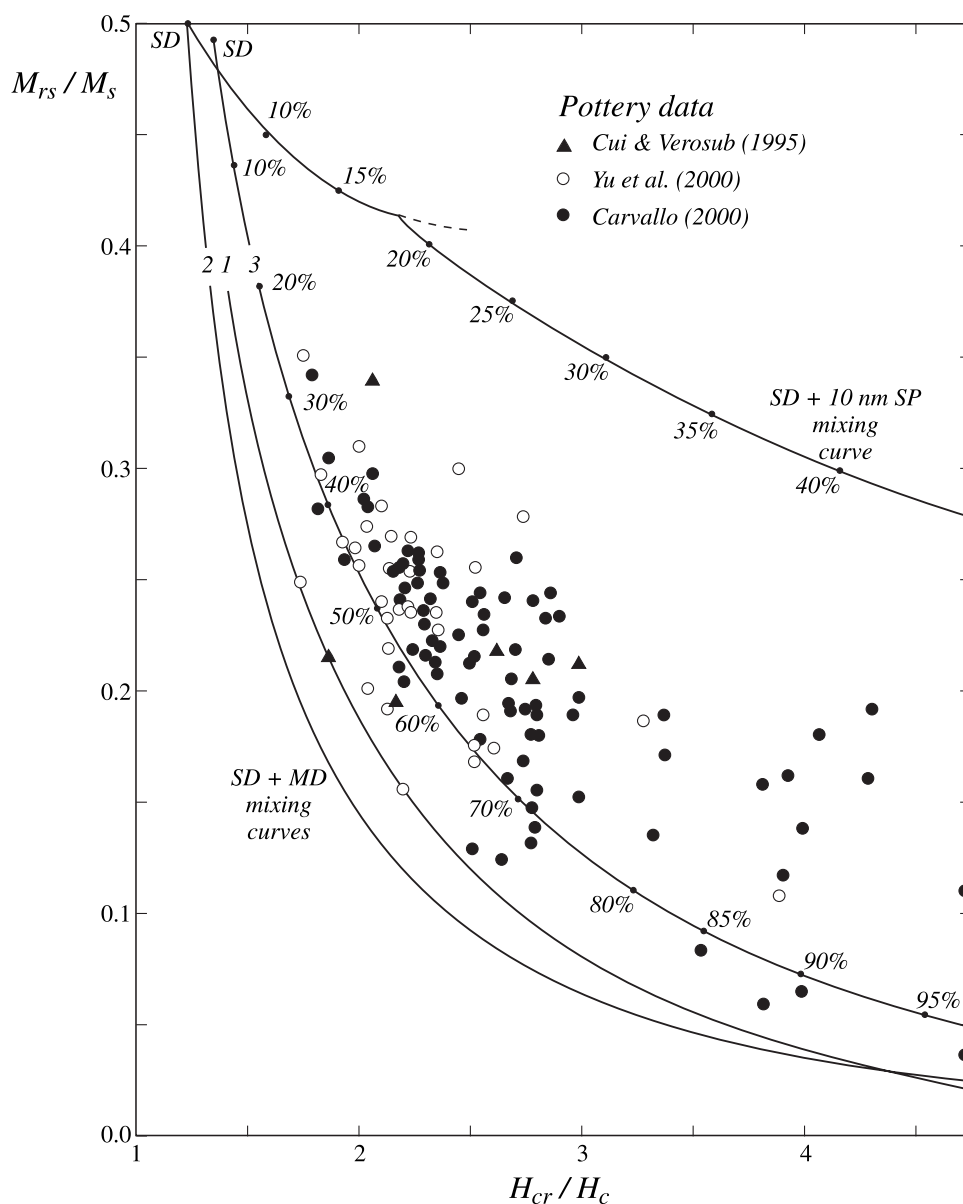
Figure 2. Hysteresis ratios for pottery samples compared to theoretical SD + MD and SD + 10-nm SP mixing curves. Numbers along the curves are volume fractions f_{MD} or f_{SP} of the soft magnetic component. Parameters for calculating mixing curves 1 and 2 are given in Table 1 of paper 1. Mixing curve 3 uses data from *Parry* [1980, 1982]: $M_{rs}/M_s = 0.493$, $H_{cr} = 590$ Oe, $H_c = 430$ Oe for elongated SD magnetite (surface oxidized, $M_s = 375$ emu/cm^3 or kA/m) and $M_{rs}/M_s = 0.0375$, $H_{cr} = 250$ Oe, $H_c = 47.5$ Oe for 15-μm small MD magnetite.

by MD and possibly bimodal hysteresis values in 10–15% of Carvallo's samples.

4. Data for Loess, Paleosols, and Modern Soils

[11] There is a growing literature on the rock magnetic properties of the loess-paleosol sequences of the Chinese loess plateau and their correlation with paleoclimate [*Heller and Evans*, 1995]. Sets of M_{rs}/M_s and H_{cr}/H_c data are scarce, however. The data in Figure 3 come from the Xifeng section, central loess plateau [*Liu et al.*, 1992] and the Luochuan section, eastern loess plateau [*Fukuma and Torii*, 1998], both spanning several successions of loess and palesols.

[12] The distribution of points in Figure 3 is unusual: M_{rs}/M_s is contained between limits 0.12 and 0.18, while H_{cr}/H_c ranges more widely, from 2.5 to 5. The Xifeng and the Luochuan loess and

paleosol data form three separate groups. All three roughly parallel the trend of SD + MD mixing curve 3, but they are offset by different amounts toward the SD + 10-nm SP mixing curve.

[13] Magnetic grain sizes within groups are narrowly distributed compared to the pottery samples of Figure 2. The Luochuan paleosols seem to have the finest sizes (small H_{cr}/H_c, above average M_{rs}/M_s) and are most nearly compatible with magnetite PSD model curves. The Xifeng loess data deviate most from the model curves. Their high H_{cr}/H_c values could be due to an admixture of fine SP grains or to a bimodal mixture with coarser MD grains. Both types of mixtures could produce constricted hysteresis loops [*Tauxe et al.*, 1996; *Fukuma and Torii*, 1998], although such loops are not mentioned by *Liu et al.* [1992].

[14] The general distribution of points in Figure 3 accords with the expectation that loess contains a heterogeneous mixture of phases with varying grain sizes, whereas paleosols are domi-
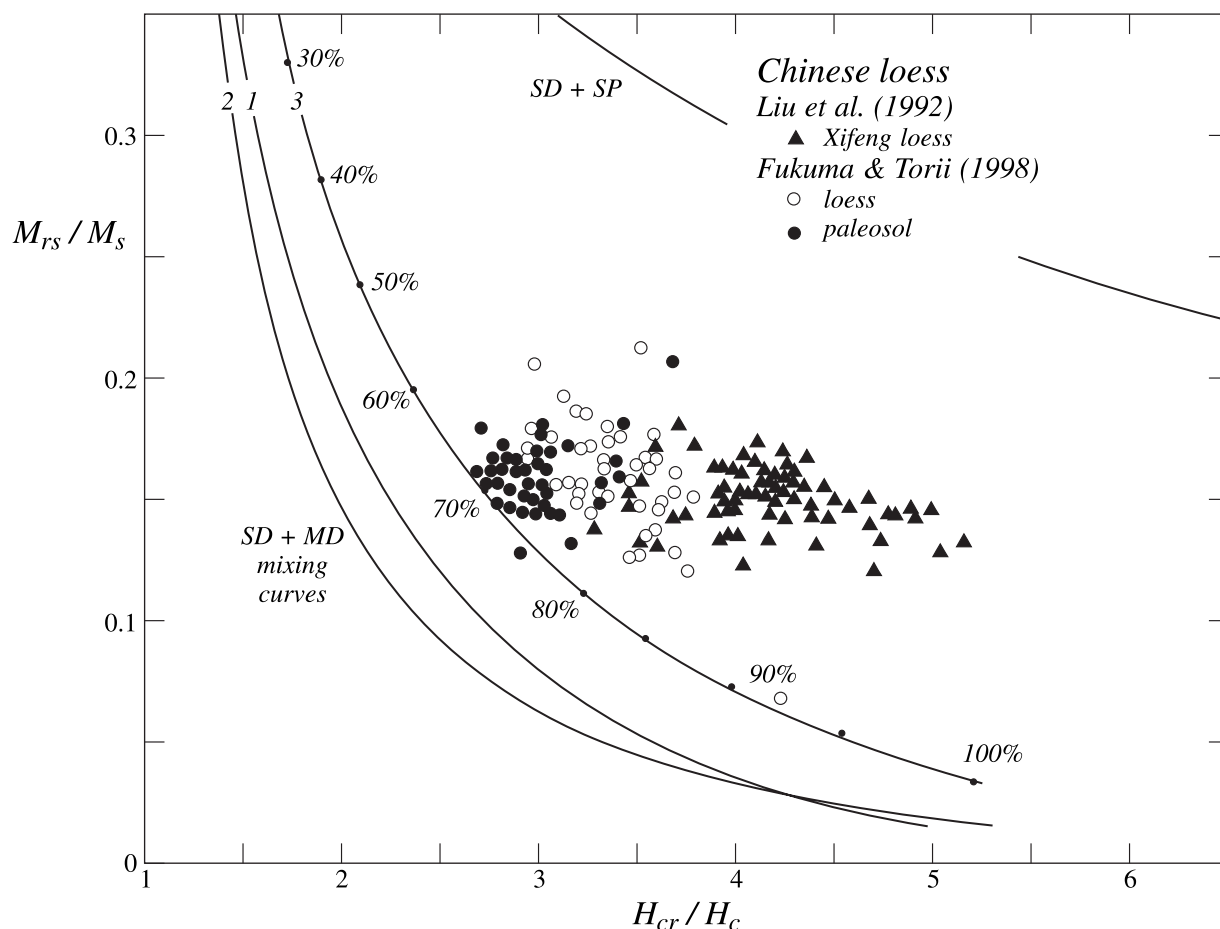
Figure 3. Data for samples from the Chinese loess plateau compared with theoretical mixing curves. The model SP size is 10 nm. Paleosol data cluster close to SD + MD mixing curve 3 around f_{MD} = 70%. Loess data are more dispersed and spread toward the SP + SD region.

nated by pedogenic magnetic material. However, the tightly grouped paleosol data give no indication of the expected pedogenic SP fraction. As well as magnetite, hematite and maghemite occur in loess and paleosol. Hematite, even in quite large grain sizes, has M_{rs}/M_s values of 0.5–0.6 and H_{cr}/H_c values of 1.5–2 that mimic those of SD magnetite [*Dunlop*, 1971; *Dankers*, 1978]. Typical hysteresis values of maghemite are less well known but probably do not differ seriously from those of magnetite of similar grain size. Neither mineral can readily explain the distributions in Figure 3.

[15]   Figure 4 shows hysteresis measurements for modern soils by *Özdemir and Banerjee* [1982]. The topsoil data lie on or near the magnetite SD + MD mixing curves, while the subsoil data may be on a parallel but higher trend. Magnetic separates have higher M_{rs}/M_s values than the bulk soils and, in the case of the subsoil, lower H_{cr}/H_c values as well. More full sets of hysteresis measurements for soils are clearly needed.

5.   Data for Lake, Shallow Marine, and Pelagic Sediments

[16]   The Day plot for magnetite-bearing sediments from Long Lake, Minnesota (Figure 4), are of special interest because *King et al.* [1982] used these samples to test methods of granulometry. Comparison of anhysteretic susceptibility χ_{ARM} and ordinary susceptibility χ [*Banerjee et al.*, 1981] leads to the conclusion that the magnetic grain size is coarse in the depth interval 897–1129 cm, medium to coarse in the interval 759–795 cm, and rapidly varying from medium to fine and back to coarse from 798 to 894 cm. The position of sample points on the Day plot correlates perfectly with the size proposed from the ratio χ_{ARM}/χ, as King et al. noted. Samples 759 and 774 have M_{rs}/M_s and H_{cr}/H_c values characteristic of intermediate PSD grain sizes, while samples 970, 1012, 1072, and 1114 have lower M_{rs}/M_s and higher H_{cr}/H_c values, approaching those of MD grains. In the interval of rapidly changing grain size, there is a one-to-one correlation between M_{rs}/M_s and χ_{ARM}/χ values. Both methods agree that the 831-cm sample has the finest grain size and approaches SD behavior.

[17]   An unusual feature of the Long Lake sediments is that their Day plot points follow very closely the SD + MD mixing curves based on pure, narrowly sized magnetites. Only the finest grain sizes (samples 816, 831, 846, 855, and 861) have points displaced significantly toward the SP + SD mixing curve.

[18]   The considerable variations in grain size at different depths seen in Long Lake sediments are almost absent in sediments from Lake Pepin, Minnesota (Figure 5). Points on the Day plot cluster in a narrow range of M_{rs}/M_s and H_{cr}/H_c over 12 m of continuous coring. Nevertheless, *Brachfeld and Banerjee* [2000a] were able to distinguish five grain-size groupings on the basis of a number of magnetic parameters, including H_c, M_{rs}/M_s, and anhysteretic remanence ratio M_{ar}/M_{rs}. These groups are distinct on the Day plot also. Even these fairly subtle size variations are important in relative paleointensity determinations [*Brachfeld and Banerjee*, 2000a]. All groups are in good agreement with theoretical magnetite SD + MD
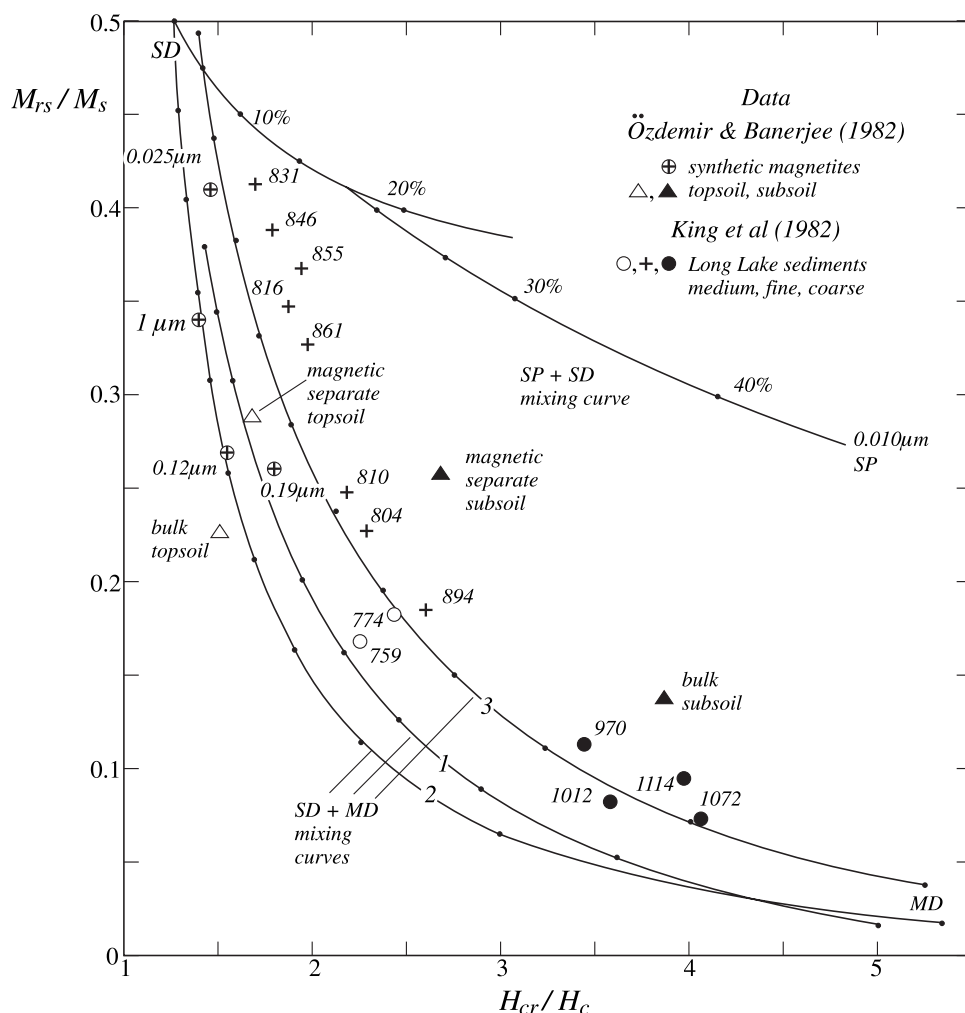
Figure 4. Hysteresis data for Minnesota soils and lake sediments compared to theoretical model curves. Except for subsoils, the data are generally compatible with SD + MD mixing curves. The progression down core in the Long Lake sediments from medium to fine to coarse grain sizes is reflected faithfully in the progression of points from mid-PSD to near-SD to near-MD along mixing curve 3 (the sample numbers correspond to stratigraphic depth in cm).

mixing curves. Only for the shallowest samples, with slightly finer magnetic grain sizes, is there any displacement of points toward the SP region of the Day plot.

[19] Glaciomarine sediments from the Palmer Deep, Antarctic Peninsula (Figure 6), have a broader distribution of points on the Day plot, both along the SD + MD mixing curves and above and to the right of the curves. In the top 600 cm of the core, samples with high susceptibility χ tend to have more MD-like values of M_{rs}/M_s and H_{cr}/H_c than low-χ samples. Samples from below 600 cm (triangles) have distinctly finer grain sizes. These evident grain-size differences complicate the use of χ as a paleoenvironmental indicator. It is also probable that there are wide size variations at any particular depth, judging by the displacement of points in the intermediate PSD range toward the SD + 10-nm SP mixing curve. The magnetic material may have more than one source.

[20] Glaciomarine sediments from McMurdo Sound, Antarctica [*Sagnotti et al.*, 1998] (Figure 7), also have zones of high and low magnetic intensity (remanences as well as χ). The higher-intensity samples in this case have points that cluster well along SD + MD model curves in the intermediate PSD region. Lower-intensity samples, like those from the Palmer Deep core, are more scattered on the Day plot, and many points are substantially displaced from the SD + MD curves, perhaps indicating an underlying second magnetic source that is hidden in strongly magnetized samples.

Whether these displaced points are due to SP + SD + PSD continuous size distributions or to disjoint SD + large MD mixtures is uncertain.

[21] Also shown in Figure 7 are remarkably tightly clustered points from pelagic sediments (Ocean Drilling Program Site 805C, Ontong Java Plateau, equatorial Pacific Ocean [*Smirnov and Tarduno*, 2000]). Magnetite is associated with fossil magnetosomes from magnetotactic bacteria, accounting for the narrow size distribution and parallelism of points with SD + MD model curves for well-sized magnetites. There is a significant difference between the distributions of points for samples above and below the Fe-redox boundary, which may be related to bacterial reduction of iron. Magnetite of this origin does not have as tight a size distribution as magnetosome magnetite [*Bazylinski and Moskowitz*, 1997]. Preferential dissolution of fine-grained magnetite below the redox boundary may also play a role [*Tarduno*, 1995].

6. Remagnetization of Carbonate Rocks

[22] Much current interest in Day plots is an outgrowth of work by *Jackson* [1990] and *Channell and McCabe* [1994] on remagnetization of limestones and dolomites. Figure 8 compares some of their data with theoretical mixing curves. The gray-white Maiolica limestones (northern Italy), which bear a primary natural
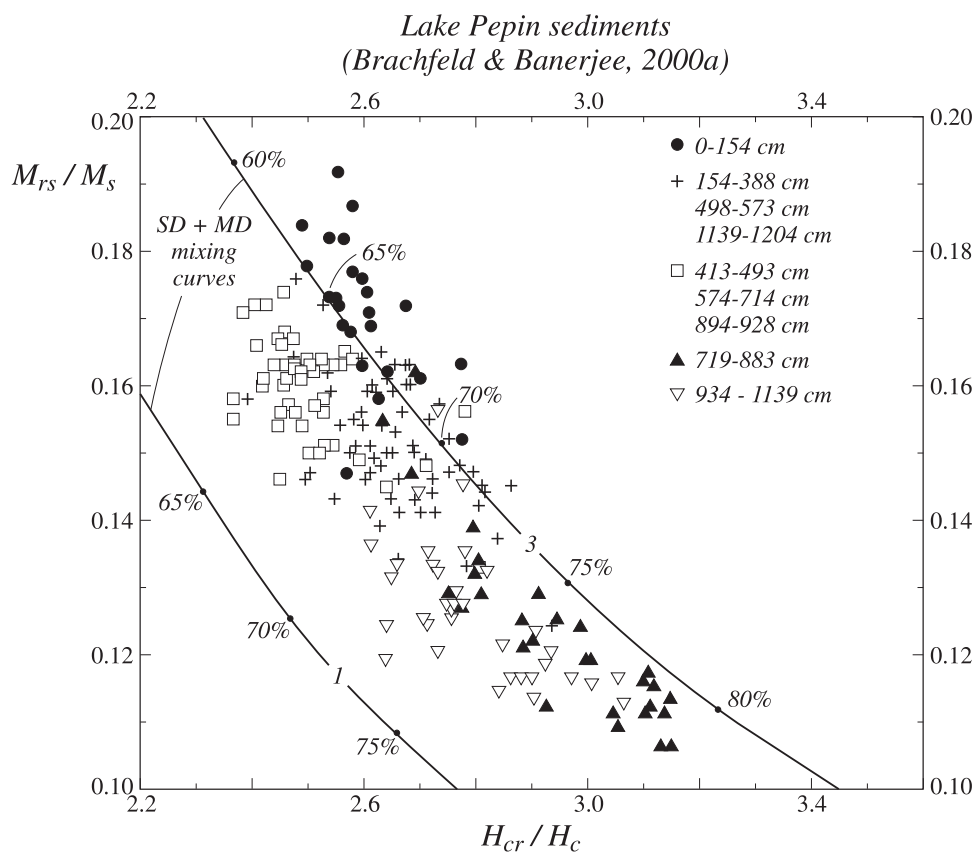
Figure 5. M_{rs}/M_s and H_{cr}/H_c data for sediments from Lake Pepin, Minnesota, fall between SD + MD theoretical curves with a narrow range of f_{MD} from ~60 to 80%. Different symbols represent core intervals with different grain sizes, judging by coercivity and ARM data. The same trend in magnetic grain size is indicated by data groupings on the Day plot.

remanence (NRM), have a rather different distribution of points on the Day plot than remagnetized limestones from the Craven Basin (U.K.) and North America, including the Onondaga and Trenton limestones and Knox dolomite of *Jackson* [1990]. Jackson proposed that SP grains were responsible for the unusual distribution of points for remagnetized carbonates. His hypothesis is borne out by the theoretical SP-SD mixing curves, each of which merges, for small SP volume fractions, with a common envelope representing SP saturation. Jackson's and Channell and McCabe's best fit lines through their data are parallel to the mixing curves for 10- and 15-nm SP particles. The mean particle sizes for best fit are ~9 and ~12 nm for the two data sets.

[23] There are several remarkable features in the remagnetized limestone data. First, there is relatively little spread in SP particle size in either study and little overlap in size between the two studies. Whatever process generates these SP particles, it produces particles of essentially a single size in a given rock. Second, there is a complete lacuna between 15 nm and the SP-SD threshold size of ~25 nm, where one might have anticipated a continuous distribution up to and beyond SD size. Some process is operational that produces ~10-nm particles unrelated to the SD grains which form the zero tiepoint anchoring all the SP-SD curves. Third, massive amounts of SP material are present. SP volume fractions of 25–75% are indicated, which in view of the tiny volume of individual SP particles implies enormous numbers of particles.

[24] *Suk et al.*'s [1993] data for the Onandaga and Trenton limestones (Figure 9) confirm *Jackson*'s [1990] measurements. However, fine-grained extracts from the same rocks have entirely different properties. Their hysteresis parameters are compatible

with PSD or SD + MD mixing curves. This material cannot be the source of SP behavior of the whole rocks.

[25] *Xu et al.*'s [1998] data for Leadville, Colorado, dolomites and limestones fall between, and subparallel to, SD + MD and SD + 10-nm SP curves (Figure 9). These are likely mixtures of PSD and SP grains (see Figure 4 of paper 1). If so, SP + PSD modeling (dot-dashed curves) suggests PSD grains in the 40–60% range on the SD + MD curve as tie points. A less likely possibility is ternary mixtures of SP + SD + MD grains, all with nonoverlapping size distributions.

[26] When *McCabe et al.* [1983] discovered polycrystalline magnetite spherules in remagnetized limestones and dolomites from New York and Missouri, it seemed probable that these diagenetic spherules were the carriers of the NRM overprint. This is not the case, however, as the magnetic extract point in Figure 9 shows and more detailed studies by *Suk and Halgedahl* [1996] confirm. M_{rs}/M_s and H_{cr}/H_c data for whole rock samples of the remagnetized Onondaga, Helderberg, and Trenton limestones (New York) fall on or close to the SD + 10 nm SP mixing curve in Figure 10, but individual spherules extracted from these rocks and from the unremagnetized Wabash limestone (Indiana) fall along the PSD and MD model curves of paper 1.

[27] The spherule data are of particular interest because they extend to sufficiently low M_{rs}/M_s and high H_{cr}/H_c values to delineate the theoretically predicted elbow between the PSD and MD curves (see Figure 1). This break in the data trend was recognized by *Suk and Halgedahl* [1996], but its significance was unclear. The M_{rs}/M_s and H_{cr}/H_c values in the MD region are comparable in some cases to those of millimeter-size single crystals of magnetite and demonstrate that at least some spherules must be monocrystalline.
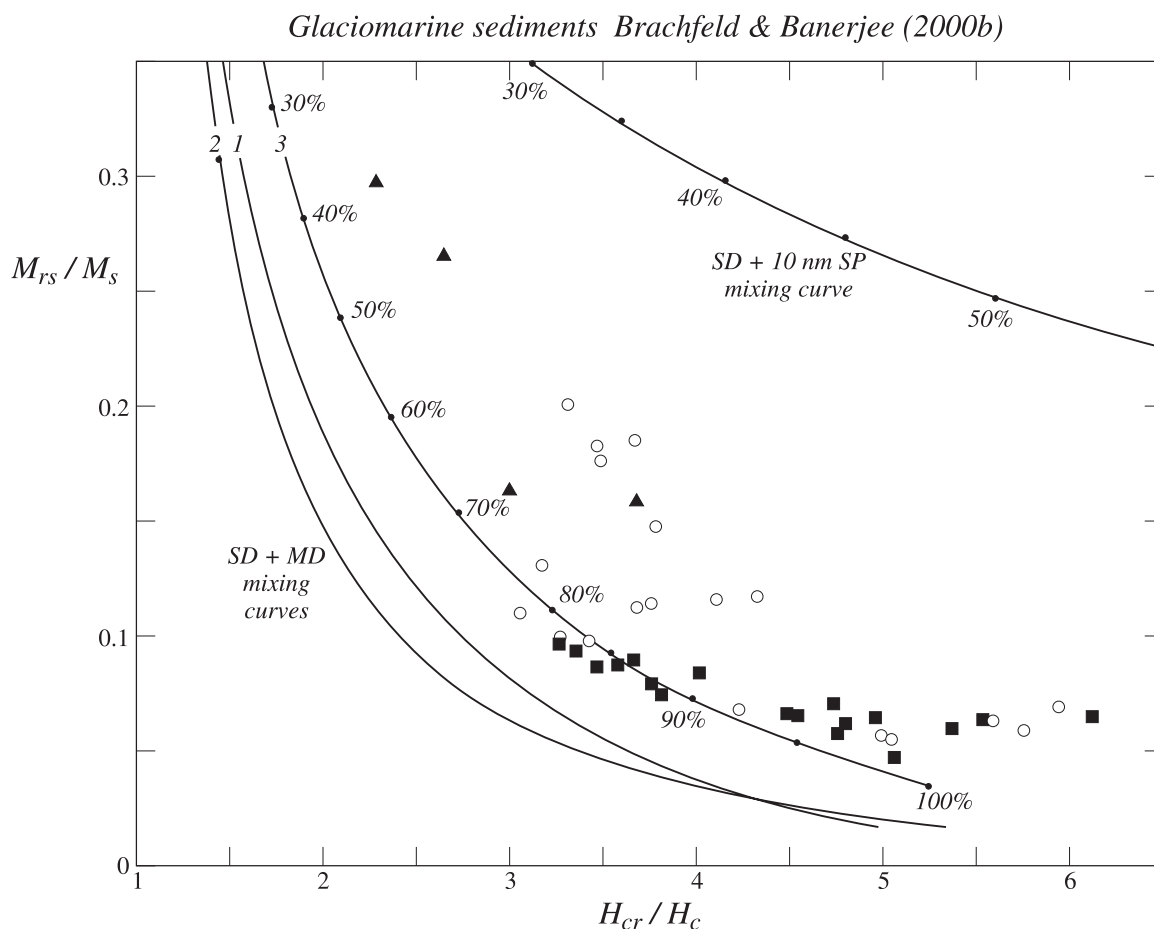
Figure 6. Day plot theoretical curves and data for Antarctic glaciomarine sediments. Strongly magnetic samples (solid squares) tend to fall along SD + MD mixing curve 3, while weakly magnetic samples (open circles) are displaced toward the SD + 10-nm SP mixing curve.

[28] Although fluids driven orogenically across basins may have caused much of the Laramide and Alleghenian-Hercynian remagnetization of North American and adjacent European carbonate rocks, there are other competing processes. Burial diagenesis of clay minerals, producing chemical remanence (CRM), is one such process [*Katz et al.*, 1998]. An example of data from the Vocontian Trough (SE France) [*Katz et al.*, 2000] is given in Figure 11. In moving eastward from Berrias to Blegiers, deeper levels of the basin are exposed, burial temperature and diagenesis increase, and smectite is increasingly replaced by illite and chlorite. Secondary CRM accompanies the clay diagenesis and anticorrelates with smectite content.

[29] In the Day plot (Figure 11), samples from Berrias have points close to and paralleling the SD + MD mixing curves. Samples with smectite and no CRM are displaced farther from these curves, and samples with CRM and no smectite are displaced still farther, some all the way to the SD + 10-nm SP mixing curve. Both Blegier samples fall close to the SP + SD curve. *Katz et al.* [2000] make similar interpretations of their data, but a knowledge of the type curves and the percentage of the soft phase (SP or MD) along each curve makes a more quantitative diagnosis possible.

## 7. Data for Oceanic Basalts and Glasses and Intrusive and Plutonic Rocks

[30] Submarine basaltic glasses are excellent recorders of paleofield intensity [*Pick and Tauxe*, 1993]. The primary magnetic mineral in mid-ocean ridge basalt (MORB) is TM60 (titanomagnetite containing ~60 mol % Ti), but glasses contain almost pure magnetite. Glasses occur interstitially in the basalt but most plentifully as quenched glassy rims of pillows. *Tauxe et al.* [1996] noted that glasses displayed two unusual characteristics, wasp-waisted or pot-bellied hysteresis loops and Day plot points lying much above those of MORB. They explained both properties convincingly as resulting from a mixture of SD and SP grain sizes. Figure 12 illustrates their data points relative to model curves from paper 1. Although there is more scatter in SP particle size than there was for most remagnetized carbonates (Figures 8–10), the typical size indicated is ~8–10 nm. There is again an apparent gap between these very small SP sizes and the thermally stable SD size, implying that the SP particles are not a tail of the SD distribution but the two have different origins.

[31] *Tauxe et al.* [1996] explained their Day plot data by adding SD and SP magnetization curves, but in order to use a continuous size distribution, an artificially low value of 15 nm had to be imposed for the SP-SD threshold size d_c. The measured threshold, $d_c \approx 25–30$ nm [*Dunlop and Özdemir*, 1997, Table 5.1], is 5–8 times larger in grain volume, magnetic moment, and susceptibility. A mixture of SD and 25 nm SP grains would have extremely high H_{cr}/H_c values, in the range 30–100 (Figure 2 of paper 1), incompatible with Tauxe et al.'s data. One is thus forced to "remove" 15–25 nm SP grains, either by moving d_c to 15 nm or by recognizing that the actual size distribution is for some reason discontinuous and lacks grains in the 15–25 nm range. Why SP magnetites in this range should be rare compared to 25–70 nm SD grains and <15 nm
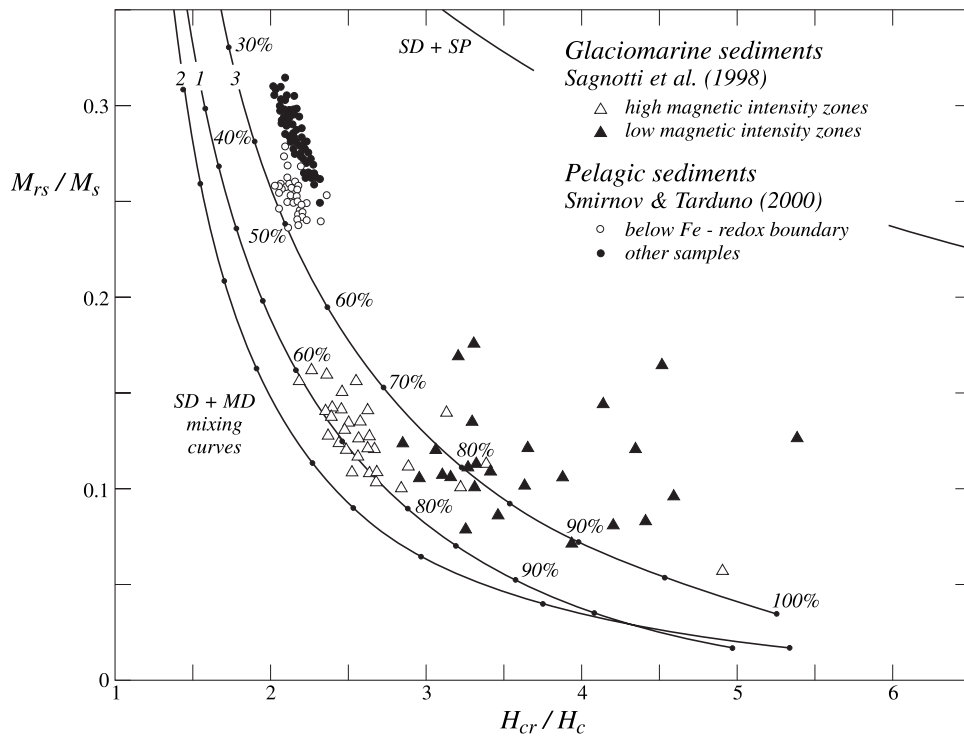
Figure 7. Day plot curves and data for Antarctic glaciomarine sediments and equatorial Pacific pelagic sediments. High magnetic intensity glaciomarine samples agree well with the theoretical SD + MD curves, while low-intensity samples scatter toward the SD + SP curve, as in Figure 6. Well-clustered groups for pelagic samples from below and above the Fe-redox boundary are distinct on the Day plot. Both data sets parallel SD + MD curve 3, with f_{MD} $\sim$35–50%.
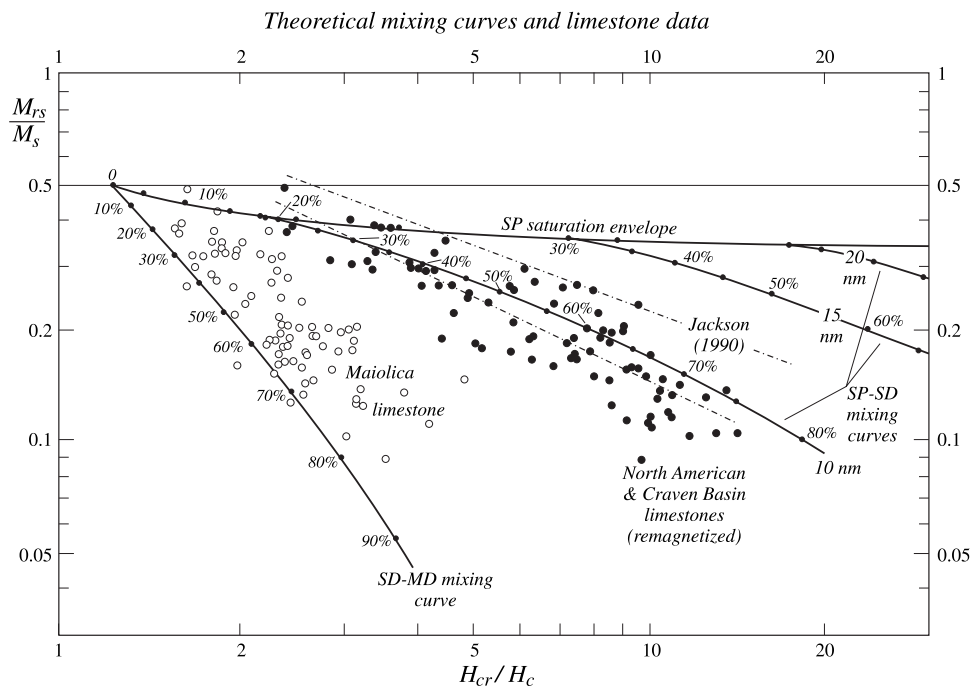

Figure 8. Hysteresis ratios for unremagnetized Maiolica limestones and remagnetized North American and Craven Basin limestones [*Channell and McCabe*, 1994] compared to theoretical curves. Unremagnetized limestone data are roughly compatible with SD-MD mixing curve 2, whereas the average (linear fit) trends of Channell and McCabe's and of *Jackson*'s [1990] data (dot-dashed lines) follow SP-SD mixing curves with average SP particle sizes of $\sim$9 and $\sim$12 nm, respectively.
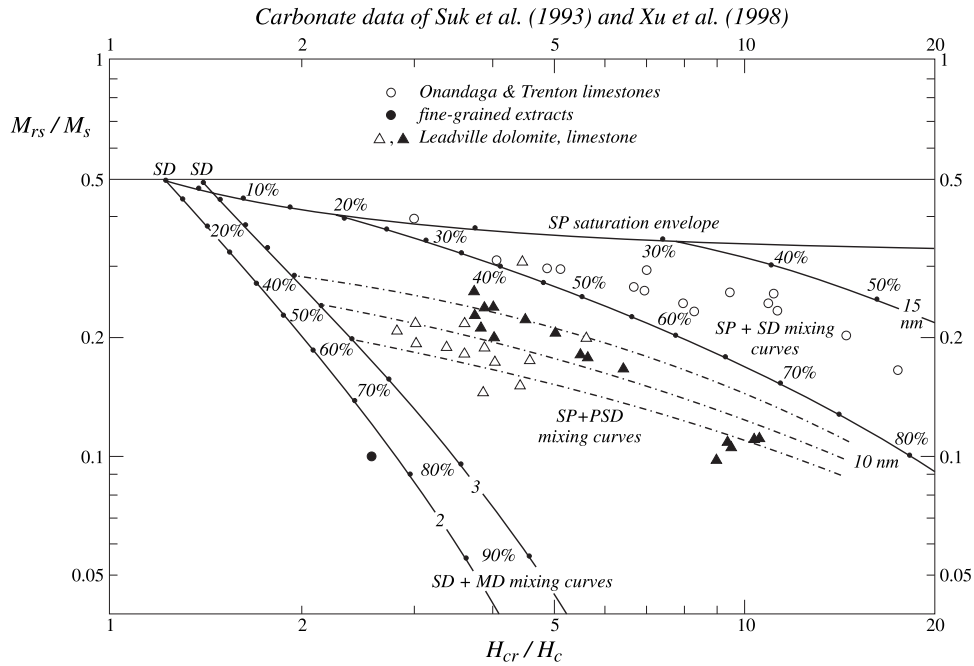
Figure 9. Day plot of data for remagnetized carbonate rocks. The Onandaga and Trenton limestone data fall between theoretical SP + SD mixing curves for SP particles sizes of 10 and 15 nm. Up to ~75% by volume of SP material is indicated, as in Figure 8. However, fine-grained extracts from these rocks have data near SD + MD mixing curves (see also Figure 10). Leadville dolomite and limestone data fall near neither set of curves but can be explained as SP + PSD mixtures (dot-dashed curves) with $f_{MD} = 40-60\%$ tiepoints on the SD + MD curve.
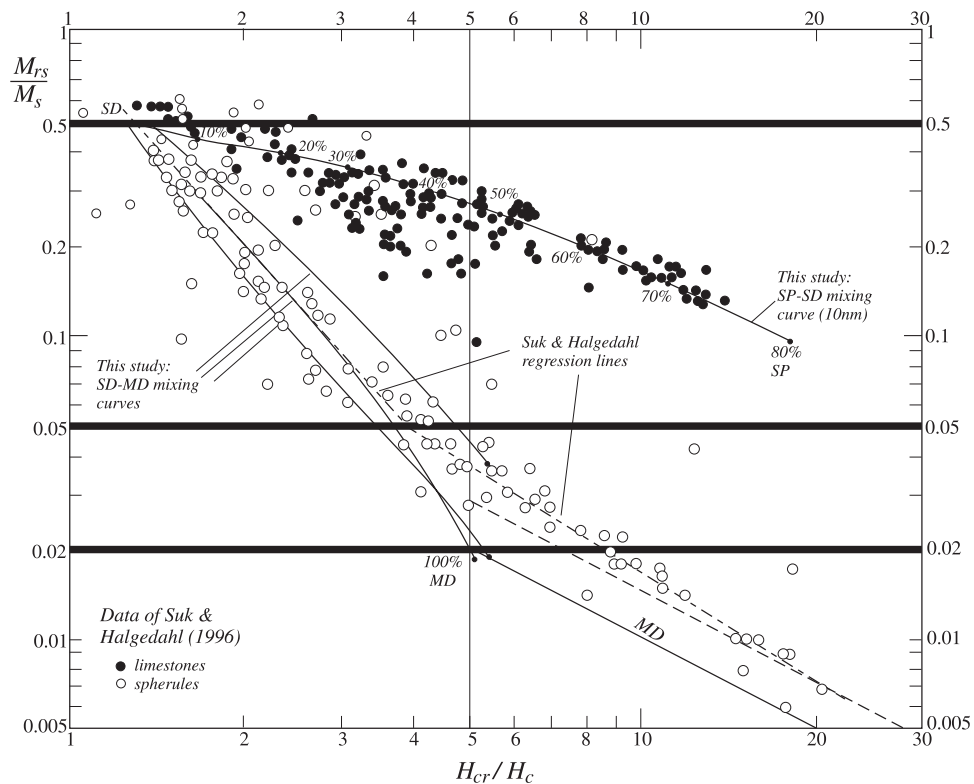
Figure 10. *Suk and Halgedahl*'s [1996] data for remagnetized limestones and magnetite spherules extracted from them. The whole rock data fall along the SD + 10-nm SP theoretical curve, as in Figures 8 and 9, but the spherule data fall along MD and SD + small MD model curves. The elbow between these trends is well indicated by the data. The dashed line is the $p = 0.15$ theoretical MD line of Figure 3 of paper 1.

*Theoretical mixing curves and Katz et al. (2000) data*
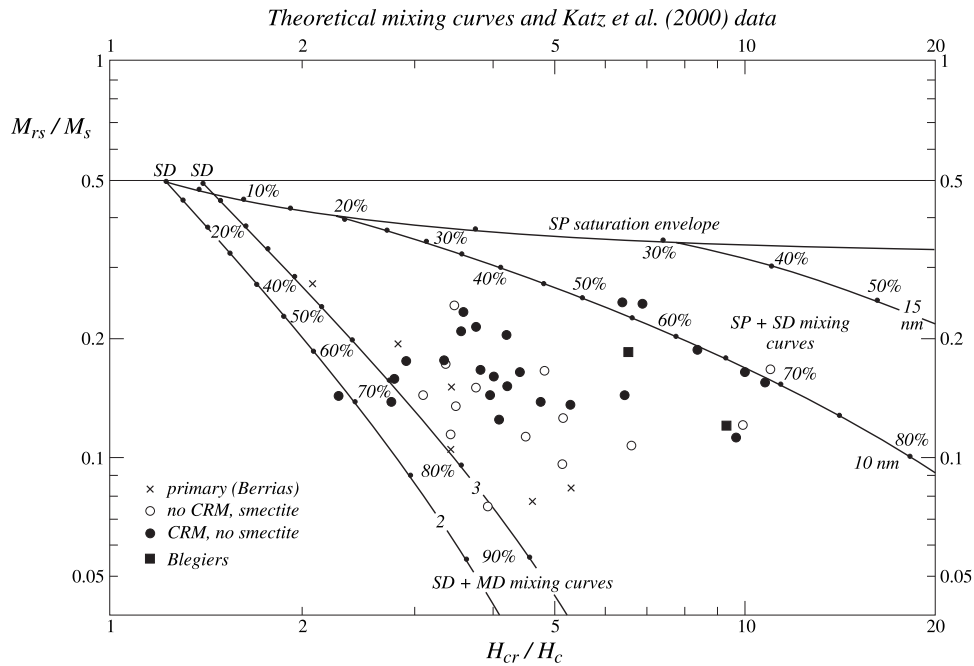
Figure 11. Data for unremagnetized (primary, no CRM) and remagnetized (CRM, Blegiers) carbonates from the Vocontian Trough compared to theoretical curves. A progressive displacement of points from the SD + MD to the SP + SD model curves accompanies increasing burial diagenesis of smectite and increasing remagnetization.

SP grains is a mystery. The same paradox has been remarked on earlier in connection with pottery, soils, and remagnetized carbonates.

[32] The nonglassy parts of basalt pillows show interesting trends of their own (Figure 13). *Soroka and Beske-Diehl* [1984] compared companion cores taken from the coarser-grained interior and the finer-grained near surface of individual pillows. In

almost all cases, lines joining pairs of points for the same pillow trend parallel to the magnetite or TM60 SD + MD mixing curves, in an upward direction consistent with finer average grain sizes toward the chilled margin of the pillow. (The mixing curves have been calculated on the assumption of purely magnetocrystalline anisotropy [*Gee and Kent*, 1995], which gives SD tie points with $M_{rs}/M_s = 0.866$ for magnetite ([111] easy axes) or 0.832 for
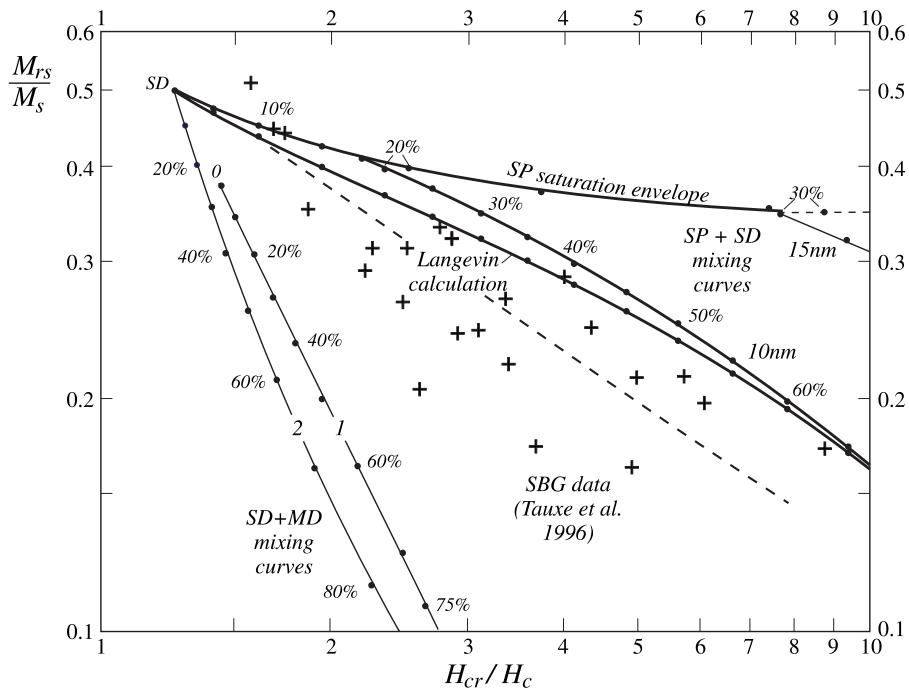
Figure 12. Hysteresis ratios for submarine basaltic glass (SBG) compared with theoretical curves. *Tauxe et al.*'s [1996] average fit to the data (dashed line) corresponds to an 8-nm SP + SD curve, and the 10-nm SP + SD curve is an upper limit to the data set.

Oceanic basalt pillows
Soroka & Beske-Diehl (1984)
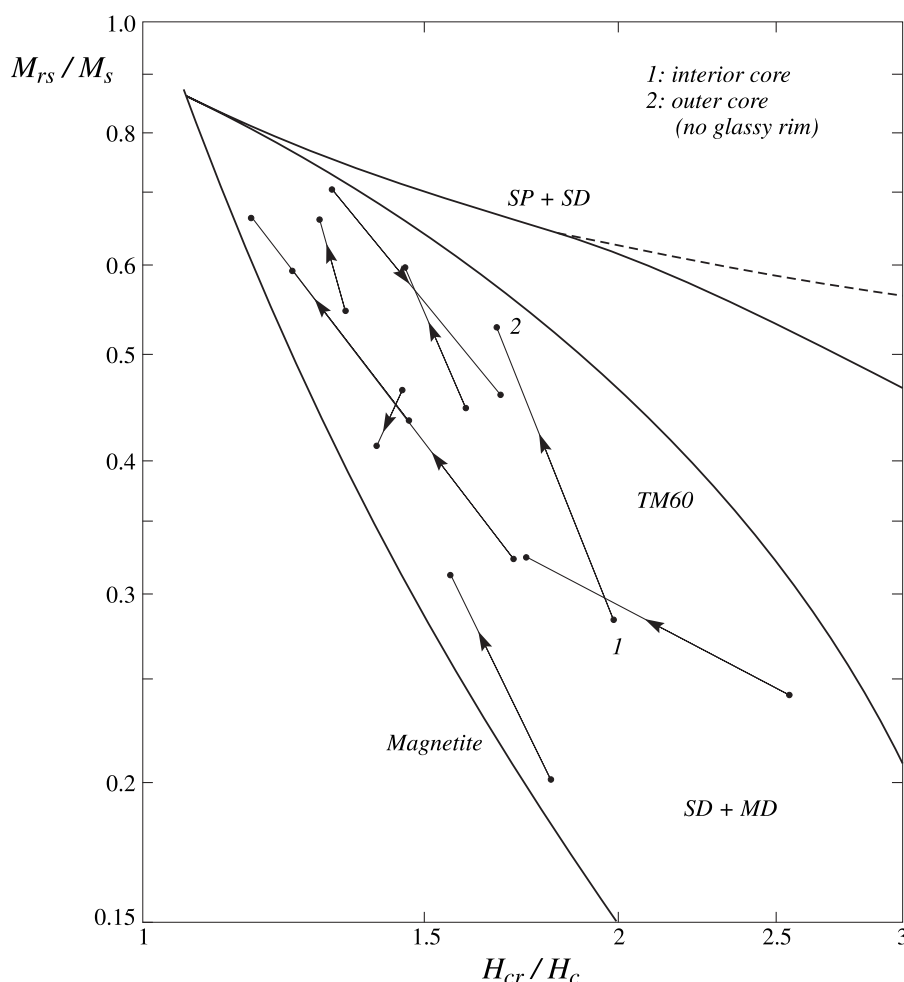
Figure 13. Comparisons of interior and outer cores from oceanic basalt pillows. In most cases, the decrease in grain size leads to a marked hardening of the hysteresis ratios. The lines joining pairs of data points are contained between magnetite and TM60 SD + MD mixing curves.

TM60 ([100] easy axes) and $H_{cr}/H_c = 1.08$.) Cooling rate is not the only factor governing grain size. Oxidation of TM60 at first produces titanomaghemite but ultimately could generate fine-grained, almost pure magnetite. The lack of transverse trends between data pairs suggests that oxidation is not a major influence in these samples.

[33] Large data sets for dredged and drilled pillow basalts from both the Pacific and Atlantic Oceans [*Gee and Kent*, 1999; *Xu et al.*, 1997] appear in Figure 14. Gee and Kent's suggested best fitting SD-MD curve through their data (dot-dashed curve) agrees very well with the calculated SD + MD mixing curve for magnetite but not at all with mixing curves for TM60, which should dominate in fresh MORB. As well as the SD + MD curve for a tie point SD value $M_{rs}/M_s = 0.832$, a second mixing curve was calculated with a tie point $M_{rs}/M_s = 0.65$, which is similar to maximum observed values in Figures 13 and 14 and would be appropriate for a mixture of crystalline and uniaxial shape anisotropies. This modified TM60 mixing curve is no more successful at fitting the MORB data.

[34] *Gee and Kent* [1999] also reported results of interior to rim traverses of a number of their pillows (Figure 15). These more detailed versions of the two-sample comparisons of Figure 13 include also subsamples within the glassy rim. The results are striking. Points from the interior to surface traverses track the

magnetite SD + MD mixing curve (PSD, decreasing average grain size) but reverse direction and track obliquely for samples near and within the glassy rim. There are two potential explanations of this "hook." The reverse track roughly follows the TM60 SD + MD mixing curves but in a direction implying increasing grain size. Neither the mineralogy nor the size progression makes sense. Gee and Kent's explanation is more reasonable: a mixture of SD and SP grains in the rim zone, with size decreasing (and thus SP fraction increasing) outward.

[35] The SP saturation envelope does not differ greatly whether M_{rs}/M_s is assumed to be 0.866, 0.832, or 0.85 (an average, since TM60 is close to the composition at which the easy axes change from [111] to [100] [*Sahu and Moskowitz*, 1995]). Because M_s and χ_{SD} are much lower for TM60 than for magnetite, the TM60 SP + SD mixing curves follow the saturation envelope for most grain sizes. However, the mixing curves for 10-nm magnetite, for either extreme of anisotropy ($M_{rs}/M_s = 0.866$ or 0.5), do have about the same trend as the rim traverse data. The ad hoc SP-SD mixing line proposed by *Gee and Kent* [1999] and shown in Figure 14 (dot-dashed curve) parallels the upper of the two SD + 10-nm SP mixing curves quite well. Thus Gee and Kent's hypothesis is reasonable.

[36] A Day plot of data for dredged dolerites, gabbros, and peridotites that originated in different layers of the oceanic crust
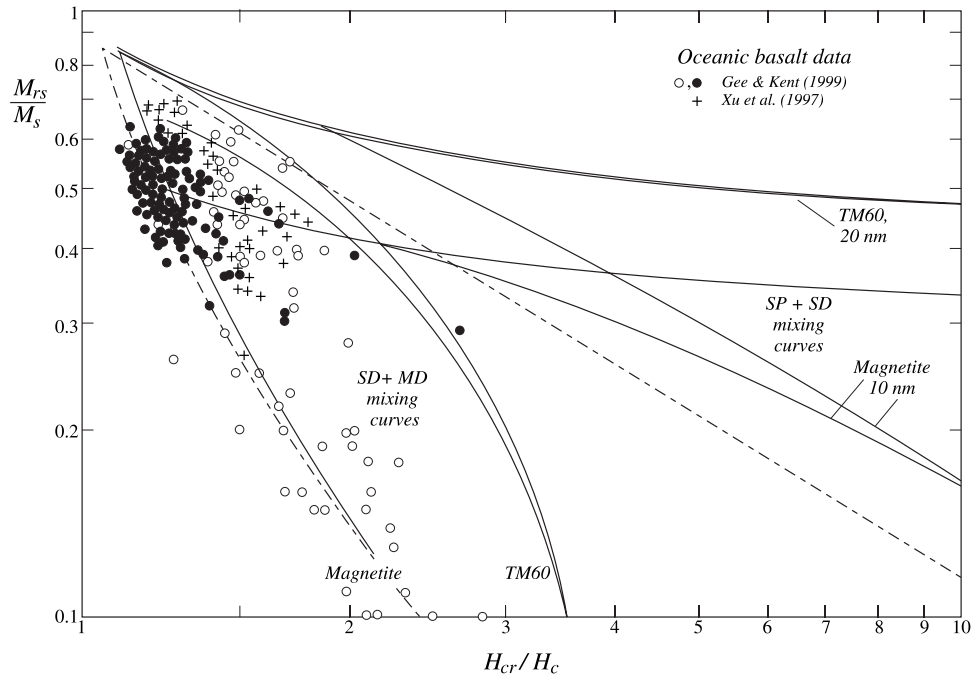
Figure 14. Large sets of M_{rs}/M_s and H_{cr}/H_c data for oceanic basalts compared to theoretical mixing curves. As in Figure 13, the data are contained between the magnetite and TM60 SD + MD mixing curves. *Gee and Kent* [1999] best fits through a subset of their basalt data and their glassy rim traverses (see Figure 15) are indicated by dot-dashed curves.

[*Dunlop and Prévot*, 1982] reveals a variety of trends depending on both rock type and serpentinization (Figure 16). Unserpentinized gabbros are weakly magnetized and owe their NRM to needle-like particles of magnetite exsolved in plagioclase [*Davis*, 1981]. Their M_{rs}/M_s and H_{cr}/H_c values follow the model magnetite SD + MD mixing curves and indicate intermediate PSD to almost SD magnetic grain sizes. All the other rock types are unusual in that their points fall below the three model mixing curves, although
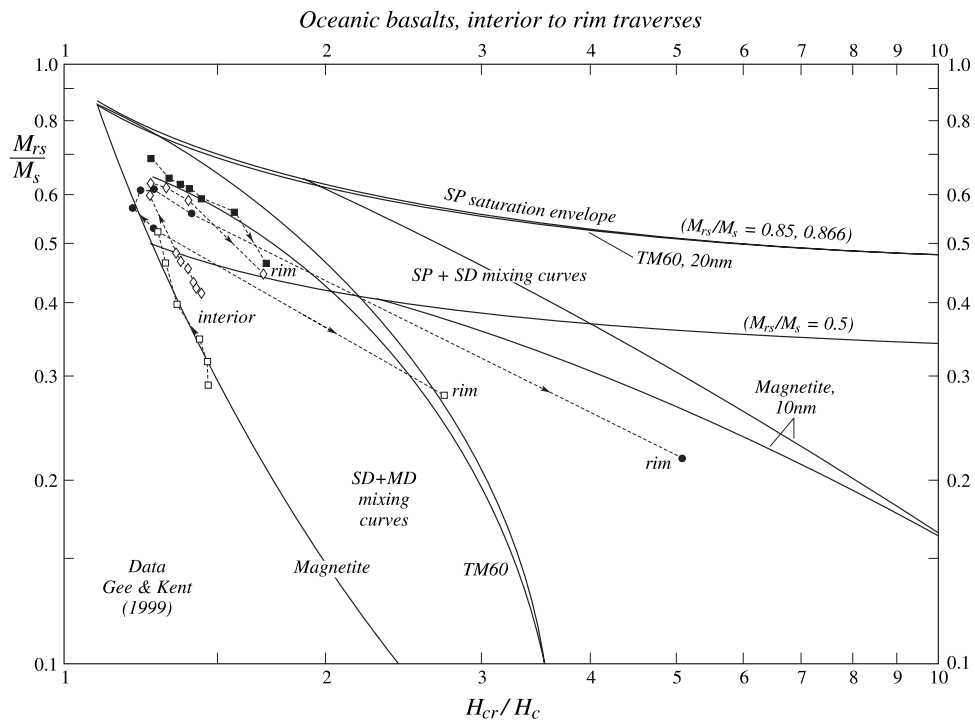
Figure 15. M_{rs}/M_s and H_{cr}/H_c results along interior to rim transverses of individual basalt pillows. As grain size decreases, the data at first track upward along the magnetite SD + MD mixing curve. Then within the glassy rims, the points reverse direction and track parallel to magnetite SD + 10-nm SP curves in the direction of increasing SP fraction (finer grain size).
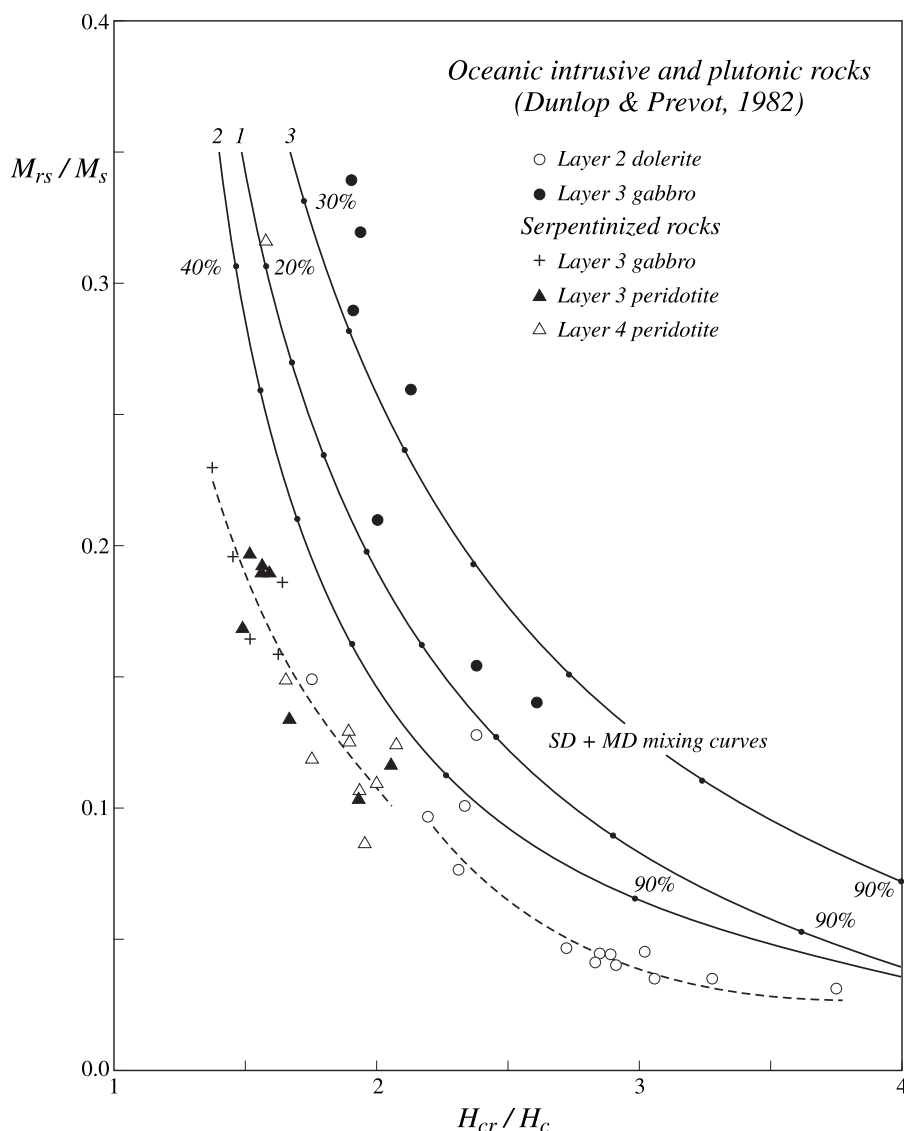
Figure 16. Day plot of data for rocks from the lower oceanic crust. Data for layer 3 gabbros, which contain exsolved needles of magnetite, follow SD + MD mixing curves quite closely, but data for the other rock types lie in a novel region below the mixing curves, with the dolerites at the coarse end of the trend and the serpentinized rocks at intermediate PSD sizes.

parallel to them. The dolerites have the coarsest grains, spanning intermediate PSD to almost true MD sizes. Serpentinized rocks, whatever their original mineralogy or crustal depth, follow a common mid-PSD trend on the Day plot. Their magnetization is due to abundant secondary magnetite produced as a by-product when olivine alters to serpentine [*Hoye and Evans*, 1975]. This magnetite is not expected to be elongate or crystallographically oriented, unlike the magnetite in plagioclase. Nevertheless, it is relatively fine grained, judging by its PSD affinities. There appear to be subtle differences in average magnetite grain size among the three serpentinized rock types, but the number of samples is too small to be certain of this.

8. Off-Curve Points on the Day Plot

[37] Points lying far to the right of SD + MD mixing curves (e.g., Figures 2, 3, 6, 7, 9, and 11) cannot be interpreted unambiguously. One possibility is broad size distributions, encom-passing PSD, stable SD and SP ranges. However, SP grains in the range $15-25$ nm (just below stable SD size) would generate values of H_{cr}/H_c from 20 to 100 (see Figure 2 of paper 1) which are not seen in the data. SP particles around 10 nm in size have appropriate M_{rs}/M_s and H_{cr}/H_c values for a ternary SP + SD + PSD mixture, but the mystery is why an otherwise continuous distribution lacks $15-25$ nm particles.

[38] A second possibility is binary mixtures of PSD and SP grains, which result in properties varying almost linearly between those of the end-members (e.g., Figure 9). The size distribution in this case must be even more disjoint: It lacks SD and smaller PSD grains as well as $15-25$ nm SP grains.

[39] The final possibility is a bimodal mixture having extreme contrast between the coercivities and/or susceptibilities of the end-members. H_c of the mixture is biased toward H_c of the soft (low-H_c or high-χ) phase, while H_{cr} is determined mainly by the hard phase. H_{cr}/H_c values can be higher than those of either end-member, displacing points on the Day plot to the right of mixing curves 1−3 (see Figure 12a of paper 1). In magnetite, however, it is difficult to produce enough contrast between end-member proper-

ties except by mixing SD and very large ($\geq$100 μm) MD grains, with no intermediate sizes.

[40] Whatever the ambiguities in interpreting points lying off standard Day plot curves, the curves themselves are a great improvement on the previous approach of sorting samples into SD, PSD, or MD (sometimes incorrectly MD + SP) "boxes" with arbitrary boundaries. The position of points within the boxes was largely ignored. Mixing curves calibrated by relative volume fractions of soft and hard phases are also useful in comparing data sets, even if it is uncertain whether individual data points are due to a single grain size, a size distribution, or two distinct sizes or distributions.

9. Conclusions

[41] The theory relating M_{rs}/M_s and H_{cr}/H_c developed in paper 1 has been applied to selected data, mostly for natural materials. The predicted elbow between PSD and MD trends on the Day plot is seen clearly in two published data sets: *Muxworthy*'s [1999] data for magnetites of a single size measured at low temperatures (Figure 1) and *Suk and Halgedahl*'s [1996] results for magnetite spherules extracted from remagnetized carbonate rocks (Figure 10).

[42] Temperature-dependent Day plot data pinpoint the MD → PSD transition size, below which SD-like moments contribute to MD remanence. This size is different above and below the Verwey transition, in accord with known changes in anisotropy and domain structure at T_V.

[43] Examples of baked clays (pottery; Figure 2), paleosols from the Chinese loess plateau (Figure 3), and modern topsoils (Figure 4), despite their diverse origins, have similar patterns on the Day plot. M_{rs}/M_s and H_{cr}/H_c values lie close to those of sized PSD magnetites (Figure 8 of paper 1) along model SD + MD mixing curves or displaced slightly toward SD + SP mixtures. The paleosols have the narrowest magnetic size distribution ($f_{MD} \approx$ 70–75%) and pottery samples have the broadest. Loess samples fall farther from PSD type curves, although the points remain well grouped.

[44] Data for sediments from two nearby lakes agree closely with predicted PSD/SD + MD model curves. In one case (Long Lake, Figure 4), known grain size trends match perfectly position along the Day plot curves. In the other (Lake Pepin, Figure 5), the size distribution is narrow, but subtle size groupings based on other magnetic properties correlate well with groups on the Day plot.

[45] Hysteresis data for glaciomarine sediments from Antarctica (Figures 6 and 7) agree well with PSD-type curves for strongly magnetic samples but are more scattered for weakly magnetic samples with heterogeneous sources of magnetic grains. Pelagic sediments from the equatorial Pacific (Figure 7) have tightly clustered points paralleling SD + MD mixing curves. Sediments containing bacterially reduced magnetite group separately from those containing only fossil magnetosomes. The resolution of the Day plot is sufficient in this case to locate the redox boundary in the sediment column.

[46] The data of *Jackson* [1990] and *Channell and McCabe* [1994] for remagnetized carbonate rocks trend along theoretical SD + SP mixing curves (Figure 8). Although the fraction of SP material is quite variable (f_{SP} from 20% to 75%), the range of SP particle sizes is narrowly constrained: 10 ± 2 nm. SP sizes between ~15 nm and the SP-SD boundary of 25–30 nm are absent. Other remagnetized carbonate data [*Xu et al.*, 1998] trend along PSD + SP mixing curves (Figure 9), rather than SD + SP curves. The best fit is again obtained for ~10-nm SP particles.

[47] Magnetite polycrystalline spherules, although secondary, are not the source of the ultrafine grains responsible for remagnetization. The extracted spherule data of *Suk and Halgedahl* [1996] follow PSD and MD model curves closely, unlike the whole rock data (Figure 10). The spherules have an extremely broad magnetic size spectrum, ranging from SD (~0.1 μm) to large MD (50–100 μm).

[48] Clay mineral diagenesis is a possible source of the magnetite that carries the remagnetization signal. Increasing burial diagenesis of smectite correlates with the appearance of CRM and displacement of M_{rs}/M_s and H_{cr}/H_c points from PSD curves to 10-nm SP + SD curves (Figure 11). A reasonable interpretation is that originally PSD-size magnetite has been increasingly supplemented by ultrafine authigenic magnetite at deeper stratigraphic levels.

[49] Submarine basaltic glass data also suggest mixtures of SD and SP magnetites (Figure 12). The SD + 10 nm SP curve is an upper bound to the data, implying a gap in the size distribution between ~15 nm and 25–30 nm, as with remagnetized carbonates. SD + 10-nm SP magnetite mixing curves likewise parallel the results of traverses within the glassy rims of MORB pillows (Figure 15).

[50] Traverses from the interiors of pillows to their surfaces follow magnetite or TM60 SD + MD mixing curves, from coarse to fine magnetic grain sizes (Figure 13). Data for pillows in general favor the magnetite rather than the TM60 curve (Figure 14), a surprising result for young MORB.

[51] Rocks from the deeper oceanic crust have hysteresis ratios compatible with magnetite SD + MD mixing curves in the case of layer 3 gabbros (Figure 16), but points for layer 2 dolerites and serpentinized gabbros and peridotites of layers 3 and 4 fall in a novel region, parallel to but below SD + MD mixing curves. The interpretation of this new region is unclear.

References

Banerjee, S. K., J. King, and J. Marvin, A rapid method for magnetic granulometry with applications to environmental studies, *Geophys. Res. Lett.*, 8, 333–336, 1981.

Bazylinski, D. A., and B. M. Moskowitz, Microbial biomineralization of magnetic iron minerals: Microbiology, magnetism and environmental science, in *Geomicrobiology: Interactions Between Microbes and Minerals, Rev. Mineral.*, vol. 35, edited by J. F. Banfield and K. H. Nealson, pp. 181–223, Mineral. Soc. of Am., Washington, D. C., 1997.

Brachfeld, S. A., and S. K. Banerjee, A new high-resolution geomagnetic relative paleointensity record for the North American Holocene: A comparison of sedimentary and absolute paleointensity data, *J. Geophys. Res.*, 105, 821–834, 2000a.

Brachfeld, S. A., and S. K. Banerjee, Rock-magnetic carriers of century-scale susceptibility cycles in glacial-marine sediments from the Palmer Deep, Antarctic Peninsula, *Earth Planet. Sci. Lett.*, 176, 443–455, 2000b.

Carvallo, C., Archeomagnetism of Ontario potsherds: Applications to the dating and orientation of pottery, M.Sc. thesis, 37 pp. + appendices 79 pp., Univ. of Toronto, Toronto, Ont., 2000.

Channell, J. E. T., and C. McCabe, Comparison of magnetic hysteresis parameters of remagnetized and unremagnetized limestones, *J. Geophys. Res.*, 99, 4613–4623, 1994.

Cui, Y., and K. L. Verosub, A mineral magnetic study of some pottery samples: Possible implications for sample selection in archaeointensity studies, *Phys. Earth Planet. Inter.*, 91, 261–271, 1995.

Dankers, P. H. M., Magnetic properties of dispersed natural iron-oxides of known grain size, Ph.D. thesis, 142 pp., Univ. of Utrecht, Utrecht, Netherlands, 1978.

Davis, K. E., Magnetite rods in plagioclase as the primary carrier of stable NRM in ocean floor gabbros, *Earth Planet. Sci. Lett.*, 55, 190–198, 1981.

Day, R., M. Fuller, and V. A. Schmidt, Hysteresis properties of titanomagnetites: Grain size and composition dependence, *Phys. Earth Planet. Inter.*, 13, 260–267, 1977.

Dunlop, D. J., Magnetic properties of fine-particle hematite, *Ann. Géophys.*, 27, 269–293, 1971.

Dunlop, D. J., Theory and application of the Day plot (M_{rs}/M_s versus H_{cr}/H_c), 1, Theoretical curves and tests using titanomagnetite data, *J. Geophys. Res.*, 107, 10.1029/2001JB000486, 2002.

Dunlop, D. J., and Ö. Özdemir, *Rock Magnetism: Fundamentals and Frontiers*, 573 pp., Cambridge Univ. Press, New York, 1997.

Dunlop, D. J., and M. Prévot, Magnetic properties and opaque mineralogy of drilled submarine intrusive rocks, *Geophys. J. R. Astron. Soc.*, *69*, 763–802, 1982.

Fukuma, K., and M. Torii, Variable shape of magnetic hysteresis loops in the Chinese loess-paleosol sequences, *Earth Planets Space*, *50*, 9–14, 1998.

Gee, J., and D. V. Kent, Magnetic hysteresis in young mid-ocean ridge basalts: Dominant cubic anisotropy?, *Geophys. Res. Lett.*, *22*, 551–554, 1995.

Gee, J., and D. V. Kent, Calibration of magnetic granulometric trends in oceanic basalts, *Earth Planet. Sci. Lett.*, *170*, 377–390, 1999.

Heller, F., and M. E. Evans, Loess magnetism, *Rev. Geophys.*, *33*, 211–240, 1995.

Hoye, G. S., and M. E. Evans, Remanent magnetizations in oxidized olivine, *Geophys. J. R. Astron. Soc.*, *41*, 139–151, 1975.

Jackson, M., Diagenetic source of stable remanence in remagnetized Paleozoic cratonic carbonates: A rock magnetic study, *J. Geophys. Res.*, *95*, 2753–2762, 1990.

Katz, B., R. D. Elmore, M. Cogoini, and S. Ferry, Widespread chemical remagnetization: Orogenic fluids or burial diagenesis of clays?, *Geology*, *26*, 603–606, 1998.

Katz, B., R. D. Elmore, M. Cogoini, M. H. Engel, and S. Ferry, Associations between burial diagenesis of smectite, chemical remagnetization, and magnetite authigenesis in the Vocontian trough, SE France, *J. Geophys. Res.*, *105*, 851–868, 2000.

King, J., S. K. Banerjee, J. Marvin, and Ö. Özdemir, A comparison of different magnetic methods for determining the relative grain size of magnetite in natural materials, *Earth Planet. Sci. Lett.*, *59*, 404–419, 1982.

Liu, X., J. Shaw, T. Liu, F. Heller, and B. Yuan, Magnetic mineralogy of Chinese loess and its significance, *Geophys. J. Int.*, *108*, 301–308, 1992.

McCabe, C., R. Van der Voo, D. R. Peacor, C. R. Scotese, and R. Freeman, Diagenetic magnetite carries ancient yet secondary remanence in some Paleozoic sedimentary carbonates, *Geology*, *11*, 221–223, 1983.

Moloni, K., B. M. Moskowitz, and E. D. Dahlberg, Domain structures in single crystal magnetite below the Verwey transition as observed with a low-temperature magnetic force microscope, *Geophys. Res. Lett.*, *23*, 2851–2854, 1996.

Muxworthy, A., Low-temperature susceptibility and hysteresis of magnetite, *Earth Planet. Sci. Lett.*, *169*, 51–58, 1999.

Özdemir, Ö., Coercive force of single crystals of magnetite at low temperatures, *Geophys. J. Int.*, *141*, 351–356, 2000.

Özdemir, Ö., and S. K. Banerjee, A preliminary magnetic study of soil samples from west-central Minnesota, *Earth Planet. Sci. Lett.*, *59*, 393–403, 1982.

Özdemir, Ö., and D. J. Dunlop, Low-temperature properties of a single crystal of magnetite oriented along principal magnetic axes, *Earth Planet. Sci. Lett.*, *165*, 229–239, 1999.

Parry, L. G., Shape-related factors in the magnetization of immobilized magnetite particles, *Phys. Earth Planet. Inter.*, *22*, 144–154, 1980.

Parry, L. G., Magnetization of immobilized particle dispersions with two distinct particle sizes, *Phys. Earth Planet. Inter.*, *28*, 230–241, 1982.

Pick, T., and L. Tauxe, Holocene paleointensities: Thellier experiments on submarine basaltic glass from the East Pacific Rise, *J. Geophys. Res.*, *98*, 17,949–17,964, 1993.

Sagnotti, L., F. Florindo, K. L. Verosub, G. S. Wilson, and A. P. Roberts, Environmental magnetic record of Antarctic palaeoclimate from Eocene/Oligocene glaciomarine sediments, Victoria Land Basin, *Geophys. J. Int.*, *134*, 653–662, 1998.

Sahu, S., and B. M. Moskowitz, Thermal dependence of magnetocrystalline anisotropy and magnetostriction constants of single crystal $Fe_{2.4}Ti_{0.6}O_4$, *Geophys. Res. Lett.*, *22*, 449–452, 1995.

Smirnov, A. V., and J. A. Tarduno, Low-temperature magnetic properties of pelagic sediments (Ocean Drilling Program Site 805C): Tracers of maghemitization and magnetic mineral reduction, *J. Geophys. Res.*, *105*, 16,457–16,471, 2000.

Soroka, W., and S. Beske-Diehl, Variation of magnetic directions within pillow basalts, *Earth Planet. Sci. Lett.*, *69*, 215–223, 1984.

Suk, D., and S. L. Halgedahl, Hysteresis properties of magnetic spherules versus whole rock specimens from some Paleozoic platform carbonates, *J. Geophys. Res.*, *101*, 25,053–25,075, 1996.

Suk, D., R. Van der Voo, and D. R. Peacor, Origin of magnetite responsible for remagnetization of Early Paleozoic limestones of New York state, *J. Geophys. Res.*, *98*, 419–434, 1993.

Tarduno, J., Superparamagnetism and reduction diagenesis in pelagic sediments: Enhancement or depletion?, *Geophys. Res. Lett.*, *22*, 1337–1340, 1995.

Tauxe, L., T. A. T. Mullender, and T. Pick, Pot-bellies, wasp-waists, and superparamagnetism in magnetic hysteresis, *J. Geophys. Res.*, *101*, 571–583, 1996.

Xu, W., R. Van der Voo, D. R. Peacor, and R. T. Beaubouef, Alteration and dissolution of fine-grained magnetite and its effects on magnetization of the ocean floor, *Earth Planet. Sci. Lett.*, *151*, 279–288, 1997.

Xu, W., R. Van der Voo, and D. R. Peacor, Electron microscopic and rock magnetic study of remagnetized Leadville carbonates, central Colorado, *Tectonophysics*, *296*, 333–362, 1998.

Yu, Y., D. J. Dunlop, L. Pavlish, and M. Cooper, Archeomagnetism of Ontario potsherds from the last 2000 years, *J. Geophys. Res.*, *105*, 19,419–19,433, 2000.

_____

D. J. Dunlop, Geophysics, Physics Department, University of Toronto, Toronto, Ontario, Canada M5S 1A7. (dunlop@physics.utoronto.ca)